SIMULATING THE SEDIMENTATION OF A DILUTE SUSPENSION

D. J. E. Harvie*, K. Nandakumar and J. H. Masliyah
Department of Chemical and Materials Engineering
University of Alberta, Edmonton, AB, Canada

November 2002

Abstract

The results of simulations of dilute suspensions of monodisperse Stokesian spheres are reported and validated against available experimental data. The equations and method of solution appear to be capable of capturing the often unstable suspension/clear fluid interface present in these systems.

Keywords: Suspensions, CFD, Sedimentation, Inclinded Settlers

1 INTRODUCTION

Sedimentation describes a process whereby solid particles are separated from a fluid, usually under the action of gravitational forces. In industrial processes sedimentation is often performed in arrays of inclinded settlers. As shown in Figure 1, an inclinded settler is a simple vessel which has its longest dimension inclined slightly away from vertical. Such vessels are popular as the production rate of clarified fluid is generally higher than the production rate of fluid from equivalently sized vertically orientated settlers, primarily because the particles have less distance to travel before impacting a wall.

For the past eight decades the performance of inclined settlers has been described using the Ponder-Nakamura-Kuroda (PNK) theory (see Davis and Acrivos, 1985). The PNK theory is a kinematic theory which gives the rate of production of clear fluid per unit depth of a rectangular vessel as

$$S = v_{\mathrm{o}} B \left[\cos\theta + (H/B)\tan\theta\right], \qquad (1)$$

where the geometric variables are as shown in Figure 1, and v_{o} is the hindered settling velocity of a single particle within the suspension region.

In practice the PNK theory often overestimates the efficiency of an inclined settler as it does not consider the kinetics of the fluid motion. When a settler is inclined, a thin layer of clear fluid forms along the underside of the longer downward facing vessel wall. As the density of this fluid is smaller than that of the nearby suspension, it experiences a large buoyancy force, causing it to accelerate upwards. Resisting this upward movement are viscous and inertial forces that act between the Clear Fluid Layer (CFL) and the adjacent wall and suspension regions. If the velocities within the CFL are large enough, waves can form along the interface that separates the CFL and suspension regions. These waves may grow and break as they ascend the vessel, entraining suspension into the CFL and decreasing the efficiency of the settler. Thus, to predict the performance of an inclined settler, we must be able to describe the formation and subsequent growth of these instabilities.

Past papers concerned the operation of inclinded settlers can be loosely classified as either analytical or numerical in nature. Studies published prior to 1985 are reviewed in Davis and Acrivos (1985) while more recent theoretical developments are outlined in Ungarish (1993).

Current analytical theories to describe the operation of inclinded settlers are generally based on the analysis presented by Acrivos and Herbolzheimer (1979) who examined the process using a simplified set of 'mixture' equations. A set of mixture equations consists of a continuity equation for each phase (ie, one for the solid and one for the fluid), a mixture averaged momentum equation to describe the movement of the suspension as a whole, and a relationship between the velocities of each phase. By neglecting inertial effects and assuming that the suspen-

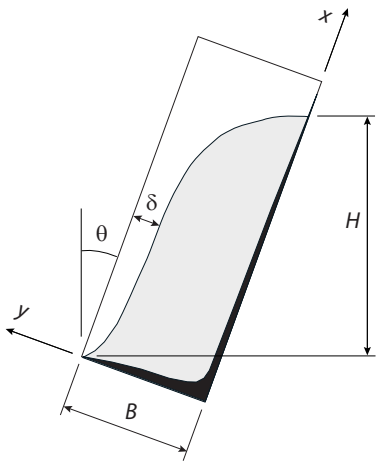

Figure 1: Sketch of an inclinded settler.

*daltonh@ualberta.ca

sion region had a uniform solids concentration, Acrivos and Herbolzheimer were able to employ a boundary layer analysis to find expressions for the geometry and flow velocities within the CFL. Further, they found that the overall sedimentation rate would be predicted by the PNK theory *provided that the interface between the suspension and clear fluid regions remained stable*. Finally, they determined that the kinetics of the sedimentation process are described by two dimensionless groups, a vessel Reynolds number and the ratio of a sedimentation Grashof number to the Reynolds number given by

$$R = \frac{H v_{\mathrm{o}} \rho_{\mathrm{f}}}{\mu_{\mathrm{f}}} \text{ and } \Lambda = \frac{H^2 g(\rho_{\mathrm{s}} - \rho_{\mathrm{f}})\phi_{\mathrm{o}}}{\mu_{\mathrm{f}} v_{\mathrm{o}}}, \qquad (2)$$

respectively, where ϕ_{o} is the assumed uniform solid volume fraction within the suspension region.

The neglect of inertia forces in Acrivos and Herbolzheimer (1979) dictates that the analysis is limited to vessels where $\Lambda \gg 1$ and $R\Lambda^{-1/3} \ll 1$ ($R\Lambda^{-1/3}$ indicates the magnitude of inertial terms in the momentum equation relative to viscous terms). Shaqfeh and Acrivos (1986) later included bulk inertial effects extending the theory to all values of $R\Lambda^{-1/3}$. Comparisons between experimental results and analytical CFL geometries predicted by these theories have generally been good, particularly so for the most viscous cases where the $R\Lambda^{-1/3}$ is small.

While the above works are able to describe the operation of inclinded settlers when the CFL interface remains stable, they do not define under what conditions this is true. Companion studies by Acrivos and co-workers have applied linear stability theory to the region surrounding the CFL interface to see under what conditions small perturbations in the position of the interface will grow. Herbolzheimer (1983) performed this analysis for low aspect ratio vessels operating under 'viscous' conditions ($R\Lambda^{-1/3} \ll 1$) and compared his findings to experimental observations of wave inception position along the interface. While the theory did not provide quantitative values of the wave inception position, he found that it did qualitatively predict trends in this parameter. In particular, his theoretical findings that wave growth was most vigorous at an inclinded angle of around 10° and that growth increases with decreases in fluid viscosity were supported by the experiments. The analysis was later applied to lower viscosity systems.

As the analytical theories apply only when the CFL interface is stable, and as the linear stability theories cannot provide quantitative information regarding this, it is evident that to predict the performance of a given settler we must turn to numerical analysis, namely Computational Fluid Dynamics (CFD). Hill *et al.* (1977) appears to have published the first CFD treatment of the settling process by simulating the settling of a very dilute suspension of mono-disperse spheres beneath an upward pointing cone. Implicit in the treatment was that the concentration within suspension region was uniform, allowing the movement of the suspension to be calculated by tracking only its interface. Hill *et al.* validated the simulations by performing experiments of the system and found good agreement between overall sedimentation times and fluid velocities, however some the aspects of the interface behaviour were poorly predicted.

More recently Laux and Ytrehus (1997) used a set of 'multi-fluid' equations to simulate the behaviour of moderately viscous sedimentation systems. Multi-fluid means that rather than using a single momentum equation to describe the average suspension movement, both fluid and solid phases use separate momentum equations. Good agreement between experimentally observed and predicted steady CFL geometries was found. Snider *et al.* (1998) used a novel Eulerian-Lagrangian method employing a set of inviscid multi-fluid equations to simulate several of the Acrivos and co-workers experiments. A simulation of one of the Herbolzheimer (1983) experiments showed the formation of waves along the CFL interface, however in contrast with the experiments, the simulations predicted that the amplitude of these waves decreased with time leading to an eventual stabilisation of the interface.

In this study we use a finite volume CFD method to simulate a variety of the mono-disperse suspension settling experiments performed by Acrivos and co-workers. The analysis is based on a set of dilute multi-fluid equations, modified to account for the small but finite solid volume fractions present in the experiments. The main emphasis of the study is on capturing the behaviour of the CFL interface, so crucial to predicting the overall performance of practical settling devices. Validation of the simulations is provided by comparing the CFL geometries observed in the experiments with those found by the model.

2 CONSERVATION EQUATIONS

Although equations describing the microscale physics of a suspension are known, due to the small local scales and shear number of particles present in such systems these equations are not useful in an engineering sense. Rather, equations in terms of averaged variables are required.

There have been several works concerned with averaging the microscale equations, however generally closure of the resulting mathematical system cannot be made without resorting to heuristic arguments. An exception to this is for a suspension of Stokesian mono-disperse spheres, where if interactions between neighbouring particles are neglected (ie, the suspension is dilute), a closed equation set can be found. Two recent studies have presented such sets. Jackson (1997), used volume averaging of the Navier-Stokes equations for the fluid phase and volume averaging of a particle momentum equation for the solid phase to derive one such set, while Zhang and Prosperetti (1997) used ensemble averaging of the same equations to find a very similar set. The minor differences between the two equation sets result from slight differences in the interpretation of the stress field surrounding an isolated particle in a Stokesian fluid, as applied to a suspension system.

Continuity Equations

$$\frac{\partial \phi_\mathrm{f}}{\partial t} + \boldsymbol{\nabla} \cdot \phi_\mathrm{f} \mathbf{u}_\mathrm{f} = 0 \text{ and } \frac{\partial \phi_\mathrm{s}}{\partial t} + \boldsymbol{\nabla} \cdot \phi_\mathrm{s} \mathbf{u}_\mathrm{s} = 0 \tag{3}$$

Momentum Equations

$$\rho_\mathrm{f} \phi_\mathrm{f} \frac{\mathcal{D}_\mathrm{f} \mathbf{u}_\mathrm{f}}{\mathcal{D}t} = -\phi_\mathrm{f} \boldsymbol{\nabla} p + 2\phi_\mathrm{f} \boldsymbol{\nabla} \mu_\mathrm{m} \mathsf{D}_\mathrm{m} - \frac{3\phi_\mathrm{s}\mu_\mathrm{f}}{4} \boldsymbol{\nabla}^2 \mathbf{u}_\mathrm{f} - \frac{3\mu_\mathrm{f}}{4} \boldsymbol{\nabla}^2 [\phi_\mathrm{s}(\mathbf{u}_\mathrm{f} - \mathbf{u}_\mathrm{s})] - \frac{9\phi_\mathrm{s}\mu_\mathrm{f}}{2a^2 F(\phi_\mathrm{f})} (\mathbf{u}_\mathrm{f} - \mathbf{u}_\mathrm{s}) + \phi_\mathrm{f} \rho_\mathrm{f} \mathbf{g} \tag{4}$$

$$\rho_\mathrm{s} \phi_\mathrm{s} \frac{\mathcal{D}_\mathrm{s} \mathbf{u}_\mathrm{s}}{\mathcal{D}t} = -\phi_\mathrm{s} \boldsymbol{\nabla} p - \phi_\mathrm{s} \boldsymbol{\nabla} p_\mathrm{s} + 2\phi_\mathrm{s} \boldsymbol{\nabla} \mu_\mathrm{f} \mathsf{D}_\mathrm{f} + \frac{3\phi_\mathrm{s}\mu_\mathrm{f}}{4} \boldsymbol{\nabla}^2 \mathbf{u}_\mathrm{f} - \frac{9\phi_\mathrm{s}\mu_\mathrm{f}}{2a^2 F(\phi_\mathrm{f})} (\mathbf{u}_\mathrm{s} - \mathbf{u}_\mathrm{f}) + \phi_\mathrm{s} \rho_\mathrm{s} \mathbf{g} \tag{5}$$

Supplementary Equations

$$\phi_\mathrm{f} + \phi_\mathrm{s} = 1 \; ; \; \mathbf{u}_\mathrm{m} = \phi_\mathrm{f} \mathbf{u}_\mathrm{f} + \phi_\mathrm{s} \mathbf{u}_\mathrm{s} \; ; \; \mathsf{D}_\mathrm{i} = \frac{1}{2} [\boldsymbol{\nabla} \mathbf{u}_\mathrm{i} + (\boldsymbol{\nabla} \mathbf{u}_\mathrm{i})^\dagger] \text{ for i} = \mathrm{f}, \mathrm{m} \; ; \; \mu_\mathrm{m} = \mu_\mathrm{f} (1 + \frac{5}{2} \phi_\mathrm{s})$$

Table 1: Conservation equations employed in this study.

The simulations performed here are based on the equations of Zhang and Prosperetti (1997), however to account for the small but finite volume fractions present in the experiments some minor modifications have been made. The equations are given in Table 1. They have a similar form to the single phase Navier-Stokes equations, however extra fluid stress, Faxen force and drag terms are present in each momentum equation. The modifications made to the Zhang and Prosperetti set are:

1. *Hindered Settling Function:* Experiments have shown that even for moderately dilute suspensions individual particles settle at speeds significantly slower than in otherwise pure fluid. A hindered settling function $F(\phi_\mathrm{f})$ has been introduced in such a manner that one-dimensional uniform concentration settling rates will be correctly predicted. The specific function employed is taken from Barnea and Mizrachi (1973).

2. *Rotational Viscous Stress:* The Zhang and Prosperetti equations include an addition viscous stress term, proportional in magnitude to the rotational 'slip' velocity between the solid and liquid phases. This stress has been neglected here as given the small moment of inertia of the particles, it is unlikely that this stress would be significant.

3. *Solid Packing Pressure:* Although modeling the sediment layer is not the primary concern of this study, it has been necessary to introduce a solid packing pressure (p_s) to support the sediment layers above the upper facing walls of the vessel. The solid pressure is taken to be a simple function of ϕ_s, negligible below $\phi_\mathrm{s} = 0.58$, but increasing sharply above this.

3 NUMERICAL METHOD

The above equations are discretised on a structured, staggered, non-uniform mesh and solved using a finite volume method. Implicit Euler time discretisations are used,

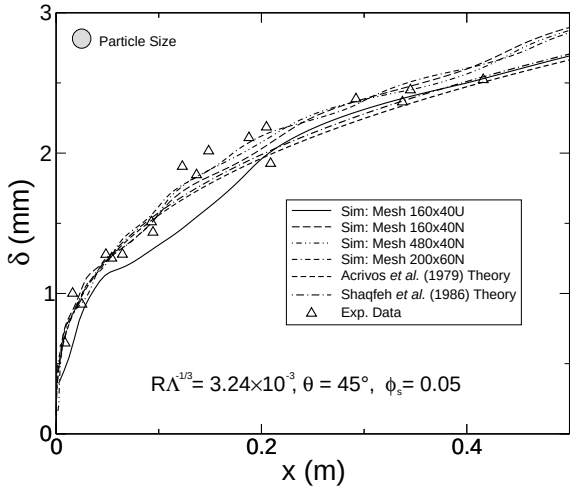

Figure 2: CFL width as a function of elevation for the low concentration Acrivos and Herbolzheimer (1979) test.

while mass and momentum advection fluxes are calculated using a multi-dimensional differencing method (Harvie and Fletcher, 2001). A Newton method is used to solve the continuity and dominant momentum terms in an inner loop, while the viscous stress and momentum advection terms are converged iteratively in an outer loop. As the drag terms tend to dominate the momentum equations in these systems, it was found necessary to solve both phase equations simultaneously in the inner Newton loop. Thus, a linear solver inverts a matrix which has twice as many terms as would be present during a single phase simulation.

4 SIMULATION RESULTS

We present simulations based on experiments reported in Acrivos and Herbolzheimer (1979), Herbolzheimer (1983) and Shaqfeh and Acrivos (1987). These experiments span a wide range of the inertial parameter $R\Lambda^{-1/3}$,

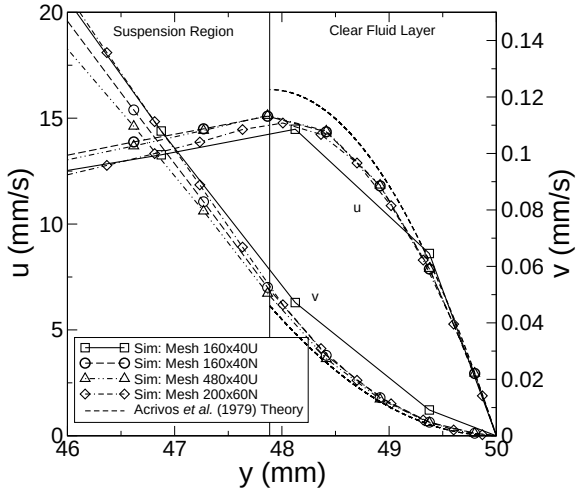

Figure 3: Longitudinal (u) and transverse (v) fluid velocities in the region of the CFL for the Acrivos and Herbolzheimer (1979) test. The position of the CFL interface is calculated using the Acrivos and Herbolzheimer theory.

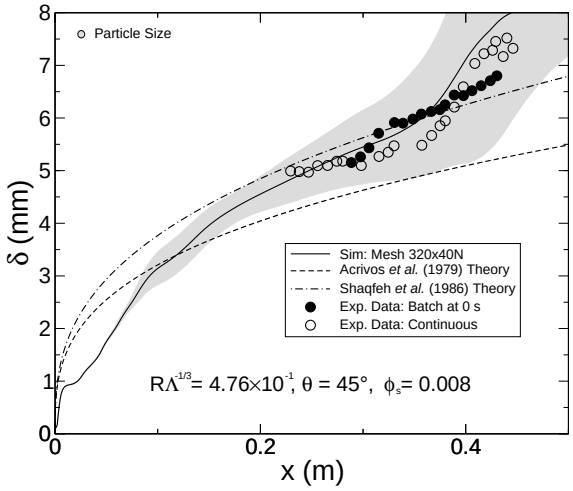

Figure 4: CFL geometry as a function of elevation for the Shaqfeh and Acrivos (1987) '1a' test. The shaded region has a width of one standard deviation of δ as it varies with time, and is centred on the mean of δ, as indicated by the solid black line. The data is based on 10 s of simulation.

from the viscous stable flows presented in Acrivos and Herbolzheimer to the nearly chaotic unstable flows shown in Shaqfeh and Acrivos.

Acrivos and Herbolzheimer (1979) Experiments: In contrast to the experiments, the simulations were performed as continuous feed tests. This was to minimise the computational expense as it allowed the effect of any changes in simulation or physical parameters to be gauged more quickly than would be the case for a batch feed test. According to the theory presented in Acrivos and Herbolzheimer (1979), for these experiments the CFL geometries for batch and continuous feed tests should be comparable. The computational domain used was setup with three ports. Suspension entered at a initial solid volume fraction of $\phi_{\rm o}$ through a large 'mass source' port in the centre of the domain, clear fluid left through a port located along the entire length of the short upper face of the vessel, and compacted sediment left through a small port at the base of the vessel, adjacent to the long upward facing wall. A two-dimensional domain having dimensions of $80\ {\rm cm}\times 5\ {\rm cm}$ was employed. A timestep of 1×10^{-3} s was used in all the simulations based on a series of timestep sensitively tests.

Figure 2 shows the calculated CFL thickness, δ, as a function of distance along the vessel wall, x (refer to Fig. 1). In calculating the simulation δ the CFL interface was approximated as the point at which $\phi_{\rm s} = \phi_{\rm o}/2$. One uniform ('U') and three non-uniform ('N') spacing meshes were tried. The CFL layer thickness converges as the as mesh is refined, indicating that the solution is for practical purposes grid independent. The predictions are close to both the experimental data and the results of the analytical theories, especially when one considers that the particle size here is relatively large, and that continuum theory results should only be interpreted over dimensions larger than those of the particles. Figure 3 shows computed fluid phase velocities within and adjacent to the CFL region at $x = 25\ {\rm cm}$. There is a difference between the maximum longitudinal velocity (u) predicted by the simulations and the Acrivos and Herbolzheimer theory. As discussed in that paper, the vessel used in the experiments was on the thinner side of the range of applicability for the theory. The theory assumes that the boundary layer created by the upwardly accelerating clear fluid is unaffected by the spacing of the plates, and this is the assumption that is violated when the vessel becomes too narrow. Thus, the difference between the simulation and analytical results may reflect the influence the opposite wall has on the CFL behaviour, however further mesh refinement studies are required to confirm this.

Figure 5 (a) shows a plot of the solid volume fraction $\phi_{\rm s}$ over the domain, computed using a 320x40N mesh. A thin black line here indicates what the equivalent PNK theory height would be for this test based on the suspension flowrate. As shown, the flow is very stable, however under close examination there appears to be a small amount of interface movement high in the vessel, above the PNK line. The upper suspension interface is not sharp here despite the suspension being mono-disperse.

Shaqfeh and Acrivos (1987) Experiments: Figures 4 and 5 (b) show the results based on the continuous feed experiment '1a' of Shaqfeh and Acrivos. A 320x40N mesh was employed and unlike previously the suspension entered the fluid domain through an inlet port located along half of the lower short face of the vessel. As in the experiments, a 'splitter' plate was used to prevent the mixing of the incoming suspension and outgoing sediment streams. The angle of inclination for this Shaqfeh and Acrivos test was the same as for the Acrivos and Herbolzheimer test, however the fluid viscosity here is significantly lower, giving a higher inertial parameter $R\Lambda^{-1/3} = 4.76 \times 10^{-1}$.

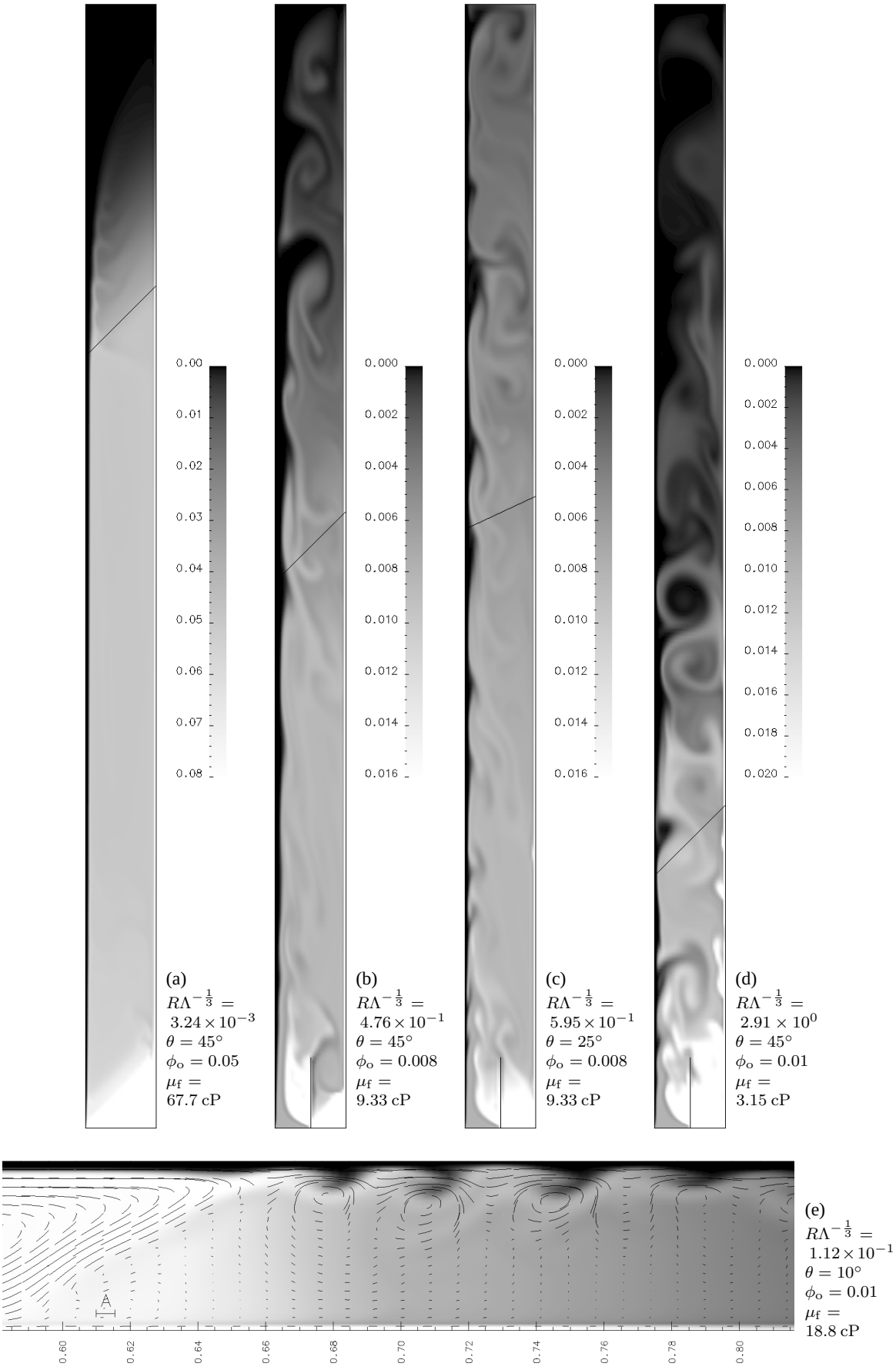

(a) $R\Lambda^{-\frac{1}{3}} = 3.24\times10^{-3}$, $\theta = 45°$, $\phi_\mathrm{o} = 0.05$, $\mu_\mathrm{f} =$ 67.7 cP

(b) $R\Lambda^{-\frac{1}{3}} = 4.76\times10^{-1}$, $\theta = 45°$, $\phi_\mathrm{o} = 0.008$, $\mu_\mathrm{f} =$ 9.33 cP

(c) $R\Lambda^{-\frac{1}{3}} = 5.95\times10^{-1}$, $\theta = 25°$, $\phi_\mathrm{o} = 0.008$, $\mu_\mathrm{f} =$ 9.33 cP

(d) $R\Lambda^{-\frac{1}{3}} = 2.91\times10^{0}$, $\theta = 45°$, $\phi_\mathrm{o} = 0.01$, $\mu_\mathrm{f} =$ 3.15 cP

(e) $R\Lambda^{-\frac{1}{3}} = 1.12\times10^{-1}$, $\theta = 10°$, $\phi_\mathrm{o} = 0.01$, $\mu_\mathrm{f} =$ 18.8 cP

Figure 5: Five inclined sedimentation simulations showing solid volume fraction ϕ_s. In Frames (a-d) a black line indicates the equivalent PNK interface height for each case. Frame (e) shows wave structures observed in the Herbolzheimer (1983) simulation. The streamlines shown in this frame were calculated by tracing massless particles across the stationary velocity field for a duration of 1 s. The dimension 'A' has a length of 10 times the one-dimensional hindered settling velocity, v_o and white represents $\phi_\mathrm{s} = 0.01$, black $\phi_\mathrm{s} = 0$..

The effect of this change is clearly indicated in Figure 5 (b) where interface waves now appear approximately halfway up the vessel. These disturbances grow to become large structures by the time they reach the top of the container. The upper suspension interface is now very poorly defined, and a large distance from the PNK line.

The geometry of the CFL is shown in Figure 4 along with corresponding analytical and experimental results. Only experimental results pertinent to the continuous operation of the settler are shown. The main computational curve in this figure is the mean of the interface position ($\delta(x)$) while the shaded area gives an indication of the amplitude of the CFL waves. Not surprisingly, the computational results suggest that the waves grow as they ascend the vessel. This is in line with the observations reported by Shaqfeh and Acrivos (1987).

The final two frames of Figure 5 are also based on the Shaqfeh and Acrivos experiments, namely experiment '3a' for Frame (c) and experiment '1d' for Frame (d). The Frame (c) experiment has a lower inclination angle than Frame (b) resulting in a decrease in the thickness of the CFL over the height of the vessel. The Frame (d) experiment has a lower fluid viscosity than Frame (b). This has a striking effect of the simulations, with large scale structures now appearing very low down in the vessel, close to the inlet port.

Herbolzheimer (1983) Experiments: Figure 5 Frame (e) shows a detailed plot of wave structures appearing in a simulation based on a Herbolzheimer experiment, namely that shown in Figure 2(c) of that paper. Here a 480x40N $1\ \mathrm{m} \times 5\ \mathrm{cm}$ mesh was used, and to replicate the experimental setup, the suspension entered the region through a 'mass source' port in the centre of the domain. The inertial parameter here lies between the two sets of experiments already considered. The interface position found was stationary for most of the vessel height, however in the dilute region above the PNK line the displayed waves appeared and their behaviour was steady with time. The streamlines shown in this figure indicate the structure of the vortices produced by the CFL flow, and show how these can entrain clear fluid back into the suspension region, harming the efficiency of the sedimenter. Note that in line with the observations of Hill (1977) the magnitude of the velocities both in the base flow and vortex regions can be over an order of magnitude larger than the equivalent hindered settling velocity for one-dimensional flow.

5 CONCLUSIONS

With the continuing increase in available computational power, CFD will become more important in the analysis of suspension flows. This study has shown that the numerics required for such computations are available, and at least in the case of dilute mono-disperse suspensions, the currently available equations of motion seem to capture the physics of these complex systems. For suspensions that are more industrially relevant, that is for more concentrated and polydisperse suspensions, there is presently little consensus about the pertinent equations, suggesting that this is where future research should be directed.

NOMENCLATURE

a	particle radius
ϕ	volume fraction
μ	absolute viscosity
ρ	density
θ	inclination angle of vessel away from vertical

Subscripts

f	fluid
m	volume averaged mixture
o	uniform concentration
s	solid

REFERENCES

Acrivos, A. and E. Herbolzheimer (1979). Enhanced sedimentation in settling tanks with inclined walls. *J. Fluid Mech.*, **92, 3**, pp. 435–457.

Barnea, E. and J. Mizrahi (1973). A generalized approach to the fluid dynamics of particulate systems. *Chem. Eng. J.*, **5**, pp. 171–189.

Davis, R. and A. Acrivos (1985). Sedimentation of noncolloidal particles at low reynolds numbers. *Ann. Rev. Fluid Mech.*, **17**, pp. 91–118.

Harvie, D. J. E. and D. F. Fletcher (2000). A new volume of fluid advection algorithm: The stream scheme. *Journal of Computational Physics*, **162, 1**, pp. 1–32.

Herbolzheimer, E. (1983). Stability of the flow during sedimentation in inclinded channels. *Phys. Fluids*, **26, 8**, pp. 2043–2054.

Hill, W. D., R. R. Rothfus and K. Li (1977). Boundary-enhanced sedimentation due to settling convection. *Int. J. Multiphase Flow*, **3**, pp. 561–583.

Jackson, R. (1997). Locally averaged equations of motion for a mixture of identical spherical particles and a newtonian fluid. *Chem. Eng. Sci.*, **52, 15**, pp. 2457–2469.

Laux, H. and T. Ytrehus (1997). Computer simulation and experiments on two-phase flow in an inclined sedimentation vessel. *Powder Technology*, **94**, pp. 35–49.

Shaqfeh, E. and A. Acrivos (1986). The effects of inertia on the buoyancy-driven convection flow in settling vessels having inclined walls. *Phys. Fluids*, **29, 12**, pp. 3935–3948.

Shaqfeh, E. and A. Acrivos (1987). Enhanced sedimentation in vessels with inclided walls: Experimental observations. *Phys. Fluids*, **30, 7**, pp. 1905–1914.

Snider, D. M., P. J. O'Rourke and M. J. Andrews (1998). Sediment flow in inclined vessels calculated using a multiphase particle-in-cell model for dense particle flows. *Int. J. Multiphase Flows*, **24**, pp. 1359–1382.

Ungarish, M. (1993). *Hydrodynamics of suspensions: Fundamentals of centrifugal and gravity separation*. Springer-Verlag.

Zhang, D. Z. and A. Prosperetti (1997). Momentum and energy equations for disperse two-phase flows and their closure for dilute suspensions. *Int. J. Multiphase Flow*, **23, 3**, pp. 425–453.